A Provably Convergent Projected Gradient-Type Algorithm for TDOA-Based Geolocation under the Quasi-Parabolic Ionosphere Model

Sen Huang, Yuen-Man Pun, Anthony Man-Cho So, *Senior Member, IEEE*, and Kehu Yang, *Member, IEEE*

***Abstract*—The problem of geolocating an unknown high-frequency emitter based on the quasi-parabolic ionosphere model with time-difference of arrival measurements of the refracted radio rays is of fundamental importance in various military and civilian applications. Such a problem admits a maximum-likelihood (ML) formulation, which is nonlinear and non-convex. By elucidating the geometry of the feasible set of the ML formulation, we develop a first-order algorithm, which we call *Generalized Projected Gradient Descent*, to solve it. We prove that every limit point of the iterates generated by our proposed algorithm is a critical point of the ML formulation. Simulation results show that our proposed algorithm can more reliably and accurately geolocate the emitter than a state-of-the-art method in various settings.**

***Index Terms*—Geolocation, ionosphere, quasi-parabolic model, time-difference of arrival, gradient descent**

I. Introduction

OWING to their ability to travel long distances, high-frequency (HF) radio waves have found many applications in both military and civilian fields [1]–[3]. In one of the earlier attempts to describe the ray path of HF radio transmission through the ionosphere, de Voogt [4] and later Croft and Hoogasian [5] proposed the quasi-parabolic (QP) model, which defines the path using a parabola-like equation in electron density versus height. The QP model provides a way to obtain the travel time of the radio signal, thereby making it possible to perform geolocation. In this paper, we consider the problem of geolocating an unknown HF transmitter using multiple coordinated distant receivers based on time-difference of arrival (TDOA) measurements of the reflected radio rays [2], [6]; cf. [7], [8]. In a recent work, Wang et al. [3] gave a maximum-likelihood (ML) formulation of the problem and proposed a three-step heuristic algorithm to solve it. However, there is no theoretical analysis of the algorithm. In particular, the work [3] neither establishes the convergence of the algorithm nor explains why the algorithm can sometimes fail to geolocate the emitter. Motivated by the above discussion, we begin by revisiting the ML formulation proposed in [3]. Our contribution is threefold. First, we describe how the geometry of the feasible set depends on the ratio between the operating frequency of the emitter and the critical frequency of the ionosphere. This sheds light on why the algorithm proposed in [3] can sometimes fail to geolocate the emitter. Second, by leveraging on our analysis of the feasible set, we reformulate the problem and design a novel first-order algorithm called the *Generalized Projected Gradient Descent* (GPGD) to tackle the resulting formulation. Third, we prove that every limit point of the iterates generated by the GPGD method is a critical point of the formulation. As our numerical results show, our proposed algorithm can more reliably and accurately geolocate the emitter than the state-of-the-art method in [3] in various settings.

S. Huang, Y.-M. Pun, and A. M.-C. So are with the Department of Systems Engineering and Engineering Management, The Chinese University of Hong Kong, Hong Kong (e-mail: {hsen, ympun, manchoso}@se.cuhk.edu.hk).

K. Yang is with the School of Telecommunications Engineering, Xidian University, Xi'an, China (e-mail: yang001@xidian.edu.cn).

II. Problem Formulation

Consider a geolocation scenario in which there is a single emitter and M sensors on the earth's surface. The location of the emitter, which we denote by $\boldsymbol{x} \in \mathbb{R}^3$, is unknown, while the locations of the sensors, which we denote by $\boldsymbol{S}_1, \ldots, \boldsymbol{S}_M \in \mathbb{R}^3$, are known. The radio-ray path between any emitter-sensor pair is assumed to travel through the ionosphere; see Fig. 1. One way of describing this path is to

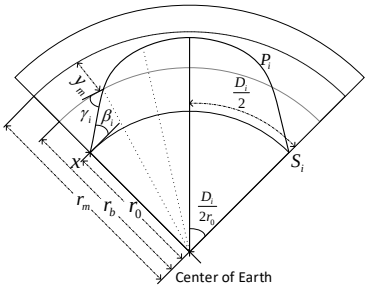

Fig. 1. Ray Path Geometry

use the QP model of the ionosphere, which relates the electron density to height using a parabola-like equation [5] and allows one to derive the geometry of the ray path. Specifically, let $r_0 \approx 6371$km be the radius of the earth, r_b be the base of the ionosphere as measured from the earth center, r_m be the distance from the earth center at which the maximum electron density is reached, and $y_m = r_m - r_b$ be layer semi-thickness. Furthermore, let f and f_c denote the operating frequency of the emitter and the critical frequency of the ionosphere, respectively, with $F = f/f_c$. Note that the parameters r_b, r_m, y_m, f_c of the ionosphere can be estimated [9], while the parameter f depends on the emitter and is assumed given. Now, for $i = 1, \ldots, M$, let $\beta_i \in [0, \frac{\pi}{2}]$ be the *flying angle* (measured above the optical horizon) of the radio ray from the emitter to sensor i and γ_i be the angle of the radio ray from the

emitter to sensor i at the base of the ionosphere. By Snell's law, one has the relation $\cos\gamma_i = \frac{r_0}{r_b}\cos\beta_i$ [5]. Moreover, by defining $A = 1 - \frac{1}{F^2} + \left(\frac{r_b}{Fy_m}\right)^2$, $B = -\frac{2r_m r_b^2}{F^2 y_m^2}$, and $C = \left(\frac{r_b r_m}{Fy_m}\right)^2 - r_0^2\cos^2\beta_i$, the distance between the emitter and sensor i along the earth's surface is given by

$$D_i(\beta_i) = 2r_0\left\{(\gamma_i - \beta_i) - \frac{r_0\cos\beta_i}{2\sqrt{C}}\times \ln\frac{B^2-4AC}{4C\left(\sin\gamma_i+\frac{1}{r_b}\sqrt{C}+\frac{1}{2\sqrt{C}}B\right)^2}\right\}, \quad (1)$$

while the group path (i.e., the signal transmit time multiplied by the speed of light c) from the emitter to sensor i is given by

$$P_i(\beta_i) = 2\left\{r_b\sin\gamma_i - r_0\sin\beta_i + \frac{1}{A}\left[-r_b\sin\gamma_i - \frac{B}{4\sqrt{A}}\ln\frac{B^2-4AC}{\left(2Ar_b+B+2r_b\sqrt{A}\sin\gamma_i\right)^2}\right]\right\}; \quad (2)$$

see Fig. 1 for an illustration and [5] for the derivation. Using sensor 1 as the reference, the (noisy) TDOA measurements are modeled as $\tau_{i1} = \tau_i - \tau_1 + n_{i1}$ for $i = 2, 3, \ldots, M$, where $\tau_i = P_i/c$ and $\{n_{i1}\}_i$ are Gaussian measurement noises with mean zero and covariance matrix $\boldsymbol{\Sigma}$. Then, one can formulate the following ML estimation problem for geolocating the emitter, where for simplicity we write $D_i = D_i(\beta_i)$ and $P_i = P_i(\beta_i)$ $(i = 1, \ldots, M)$; cf. [3]:

$$\min_{\boldsymbol{x},\boldsymbol{\beta}} \ \phi(\boldsymbol{\beta}) = (\boldsymbol{G}\boldsymbol{P} - \boldsymbol{\pi})^T\boldsymbol{\Sigma}^{-1}(\boldsymbol{G}\boldsymbol{P} - \boldsymbol{\pi})$$

$$\text{s.t.} \ \|\boldsymbol{S}_i - \boldsymbol{x}\| = 2r_0\sin\left(\frac{D_i}{2r_0}\right), \ i = 1, \ldots, M, \quad (3a)$$

$$\|\boldsymbol{x}\| = r_0. \quad (3b)$$

Here, $\boldsymbol{P} = [P_1, \ldots, P_M]^T \in \mathbb{R}^M$, $\boldsymbol{\beta} = [\beta_1, \ldots, \beta_M]^T \in \mathbb{R}^M$, $\boldsymbol{G} = \begin{bmatrix}-\boldsymbol{e}_{M-1} & \boldsymbol{I}_{M-1}\end{bmatrix} \in \mathbb{R}^{(M-1)\times M}$, and $\boldsymbol{\pi} = c\,[\tau_{21}, \tau_{31}, \ldots, \tau_{M1}]^T \in \mathbb{R}^{M-1}$, where $\boldsymbol{e}_n$ denotes the n-dimensional column vector of all ones and $\boldsymbol{I}_n$ denotes the $n\times n$ identity matrix. In this formulation, the Euclidean distance between the emitter and sensor i (where $i = 1, \ldots, M$) is given by (3a) and the emitter is constrained to be on the earth's surface by (3b). Note that due to the non-line-of-sight nature of the ray path, the above formulation is different from most existing formulations (e.g., [10]–[12]) in the localization literature. Although the formulation (3) is nonlinear and non-convex, it possesses some favorable properties that can be exploited in algorithm design. This will be explained next.

III. Problem Analysis and Algorithm Design

A. Problem Analysis

Observe that once the flying angle β_i is determined, both D_i and P_i are also determined; see (1) and (2). To better understand the structure of the nonlinear equations (3a), let us plot the function $\beta \mapsto D(\beta)$. As can be verified and also illustrated in Fig. 2, when $F \le 1$, D is monotonically decreasing and one-to-one in $\beta \in [0, \frac{\pi}{2}]$. Hence, given a value $\bar{D}$, there is a unique $\bar{\beta}$ such that $\bar{D} = D(\bar{\beta})$. On the other hand, when $F > 1$, D decreases as β increases and reaches a minimum at the angle β^{U_1}, whose value can be found by, say, the golden-section search [13]. The value $D(\beta^{U_1})$ is known as the *skip distance*. In particular, the emitter's signal cannot reach sensors whose distance from the emitter is less than the skip distance [14]. As β increases beyond β^{U_1}, D increases again until $\beta = \beta^{U_2}$, at which the ray penetrates the ionosphere and is not refracted back to the ground. The value β^{U_2} can be obtained by solving $B^2 - 4AC = 0$; see (1).

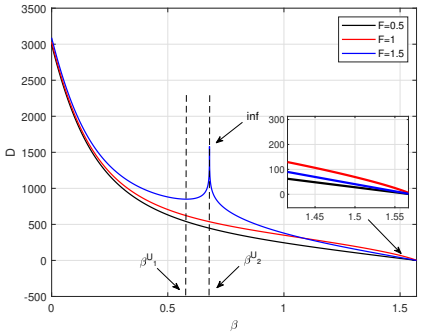

Fig. 2. Graph of $\beta \mapsto D(\beta)$

The case where $F > 1$ is often of practical interest, as the emitter could then provide certain long-range coverage capabilities [14]. However, in this case, given a value $\bar{D}$ that is greater than the skip distance, there are two corresponding flying angles—one lies in $[0, \beta^{U_1})$ and the other in $(\beta^{U_1}, \beta^{U_2})$; see Fig. 2. For most purposes, only rays of the former type are used, while rays of the latter type are considered a nuisance [14]. In view of the above discussion, we shall focus on the case where $F > 1$ in the sequel and incorporate the constraints $\beta_i \in [0, \beta^{U_1}]$ for $i = 1, \ldots, M$ into the ML formulation (3). Since β_i is a function of $\boldsymbol{x}$ by (3a), we can eliminate the variable $\boldsymbol{\beta}$ from (3) and consider the equivalent problem

$$\min_{\boldsymbol{x}} \ \theta(\boldsymbol{x}) = \phi(\boldsymbol{\beta}(\boldsymbol{x}))$$

$$\text{s.t.} \ L \le \|\boldsymbol{S}_i - \boldsymbol{x}\| \le U, \ i = 1, \ldots, M, \quad (4a)$$

$$\|\boldsymbol{x}\| = r_0, \quad (4b)$$

where $L, U > 0$ are bounds obtained from the constraint $\beta_i \in [0, \beta^{U_1}]$ and can be calculated from (1) and (3a). Although the constraints (4a) may seem non-convex at first sight, by observing that $\|\boldsymbol{S}_i\| = \|\boldsymbol{x}\| = r_0$ for $i = 1, \ldots, M$, they can be simplified to

$$2r_0^2 - U^2 \le 2\boldsymbol{S}_i^T\boldsymbol{x} \le 2r_0^2 - L^2, \ i = 1, \ldots, M, \quad (5)$$

which are *linear* inequality constraints. Hence, the main difficulty of problem (4) lies in the non-convexity of the objective function θ and the constraint (4b).

To the best of our knowledge, the formulation (4) is the first to explicitly incorporate the constraints $\beta_i \in [0, \beta^{U_1}]$ on the flying angles. Previously, Wang et al. [3] tried to control the flying angles by adding a penalty term to the objective function in (3). However, it is not clear how to choose the penalty parameter so that the flying angles will lie in the desired range.

In particular, given a current iterate $\bar{\boldsymbol{x}}$, if there are two flying angles β_i^-, β_i^+, where $0 \leq \beta_i^- < \beta^{U_1} < \beta_i^+ < \beta^{U_2}$ (see Fig. 2), that could satisfy the i-th constraint in (3a) with $\boldsymbol{x} = \bar{\boldsymbol{x}}$, the algorithm proposed by Wang et al. [3] may not rule out β_i^+. As we shall see in Section IV, this can often cause the algorithm to fail to geolocate the emitter.

B. Generalized Projected Gradient Descent Method

Given the success of the semidefinite relaxation technique [15] in dealing with a wide range of localization problems [16], [17], it is tempting to apply the technique to tackle problem (4). However, a quick inspection of the structure of the objective function θ suggests that such an approach is not straightforward. Hence, we propose to tackle problem (4) directly using a projected gradient-type method. To begin, observe that by using the chain rule and applying implicit differentiation on (3a), we have

$$\nabla\theta(\boldsymbol{x}) = 2\left(\boldsymbol{G}\frac{\partial \boldsymbol{P}}{\partial \boldsymbol{\beta}}\frac{\partial \boldsymbol{\beta}}{\partial \boldsymbol{x}}\right)^T \boldsymbol{\Sigma}^{-1}(\boldsymbol{G}\boldsymbol{P} - \boldsymbol{\pi}), \tag{6}$$

where

$$\frac{\partial \boldsymbol{P}}{\partial \boldsymbol{\beta}} = \mathrm{Diag}\left(\frac{dP_1}{d\beta_1}, \cdots, \frac{dP_M}{d\beta_M}\right) \in \mathbb{R}^{M\times M},$$

$$\frac{\partial \boldsymbol{\beta}}{\partial \boldsymbol{x}} = \begin{bmatrix} -\left(r_0 \sin\left(\frac{D_1}{r_0}\right)\frac{dD_1}{d\beta_1}\right)^{-1}\boldsymbol{S}_1^T \\ \vdots \\ -\left(r_0 \sin\left(\frac{D_M}{r_0}\right)\frac{dD_M}{d\beta_M}\right)^{-1}\boldsymbol{S}_M^T \end{bmatrix} \in \mathbb{R}^{M\times 3}.$$

Let $\mathcal{X}$ be the feasible region of problem (4). Then, we can solve problem (4) via the following algorithm:

Algorithm 1 Generalized Projected Gradient Descent (GPGD) for Solving (4)

1: **Initialization:** initial iterate $\boldsymbol{x}^0 \in \mathcal{X}$; bounds $L, U > 0$ in (4a); maximum number of iterations T.
2: **for** $k = 0, 1, 2, \ldots, T$ **do**
3: Set $\boldsymbol{x} = \boldsymbol{x}^k$ in (3a) and find the solutions $\beta_{1,k}, \ldots, \beta_{M,k}$.
4: Take the gradient step
$$\bar{\boldsymbol{x}}^{k+1} = \boldsymbol{x}^k - \alpha_k \cdot \nabla\theta(\boldsymbol{x}^k),$$
where $\alpha_k > 0$ is the step size and $\nabla\theta(\boldsymbol{x}^k)$ is computed via (6) using $\boldsymbol{x}^k, \beta_{1,k}, \ldots, \beta_{M,k}$.
5: Perform the projection
$$\boldsymbol{x}^{k+1} = \mathrm{Proj}_{\mathcal{X}}(\bar{\boldsymbol{x}}^{k+1}).$$
6: **end for**

Before we proceed further, some discussion on the implementation details of Algorithm 1 is in order. First, line 3 can be implemented using an one-dimensional search [13]. Second, the step size α_k in line 4 can be determined by a backtracking line search [13]. Third, although line 5 involves projecting a point onto the non-convex set $\mathcal{X}$, it can be tackled using an alternating projection strategy. Specifically, observe that $\mathcal{X}$ can be expressed as $\mathcal{X} = \mathcal{P} \cap \mathcal{M}$, where $\mathcal{P}$ is the polyhedron defined by (5) and $\mathcal{M}$ is the sphere defined by (4b). On one hand, the projection $\mathrm{Proj}_{\mathcal{P}}(\boldsymbol{y})$ of the point $\boldsymbol{y}$ onto the polyhedron $\mathcal{P}$ is a well-studied problem and can be efficiently solved using Hildreth's algorithm; see [18]. On the other hand, the projection $\mathrm{Proj}_{\mathcal{M}}(\boldsymbol{y})$ of the point $\boldsymbol{y}$ onto the sphere $\mathcal{M}$ is simply given by $\mathrm{Proj}_{\mathcal{M}}(\boldsymbol{y}) = r_0 \cdot \frac{\boldsymbol{y}}{\|\boldsymbol{y}\|}$. Hence, starting at the point $\boldsymbol{y}^0 = \boldsymbol{y}$, we can generate a sequence of points $\{\boldsymbol{y}^j\}_j$ via the alternating projections

$$\boldsymbol{y}^{2j+1} = \mathrm{Proj}_{\mathcal{P}}(\boldsymbol{y}^{2j}),\ \boldsymbol{y}^{2j+2} = \mathrm{Proj}_{\mathcal{M}}(\boldsymbol{y}^{2j+1}),\ j = 0, 1, \ldots.$$

It has been shown that the sequence $\{\boldsymbol{y}^j\}_j$ will locally converge to a point $\bar{\boldsymbol{y}} \in \mathcal{X}$ at a linear rate [19].

Unlike the algorithm proposed in [3], our proposed GPGD method does not require the tuning of a penalty parameter. As we shall see in Section IV, the GPGD method is more robust and can yield higher geolocation accuracy than the algorithm in [3].

Next, let us study the convergence behavior of our proposed GPGD method.

C. Convergence Analysis of GPGD

Although problem (4) is non-convex, its objective function and constraint set have nice structures. These structures would allow us to establish the convergence of the GPGD method (Algorithm 1). Specifically, we have the following result:

Theorem 1. *Let $\bar{\mathcal{X}}$ be a compact subset of $\mathrm{int}(\mathcal{P}) \cap \mathcal{M}$, where $\mathrm{int}(\mathcal{P})$ denotes the interior of $\mathcal{P}$. Then, there exists a constant $B > 0$ such that if the step sizes $\{\alpha_k\}_k$ satisfy $\alpha_k \in (0, B)$ for $k = 0, 1, \ldots$ and the iterates $\boldsymbol{x}^0, \boldsymbol{x}^1, \ldots,$ generated by Algorithm 1 all lie in $\bar{\mathcal{X}}$, then every limit point of the sequence $\{\boldsymbol{x}^k\}_k$ is a critical point of problem* (4).

Proof. Using the definition of θ and the expressions for D_i and P_i in (1) and (2), respectively, we see that θ is twice differentiable and lower bounded by 0 on $\bar{\mathcal{X}}$. This implies that θ has a Lipschitz continuous gradient on $\bar{\mathcal{X}}$. Hence, by the results in [20, Section 5], there exists a constant $B > 0$, which depends on the Lipschitz constant of $\nabla\theta$, such that if the step sizes $\{\alpha_k\}_k$ satisfy $\alpha_k \in (0, B)$ for $k = 0, 1, \ldots$ and the iterates $\boldsymbol{x}^0, \boldsymbol{x}^1, \ldots,$ generated by Algorithm 1 all lie in $\bar{\mathcal{X}}$, then the sequence $\{\theta(\boldsymbol{x}^k)\}_k$ is monotonically decreasing and tends to a limit. This, together with the Lipschitz continuity of $\nabla\theta$, implies that every limit point of $\{\boldsymbol{x}^k\}_k$ is a critical point of problem (4). □

It is worth noting that our proposed GPGD method is the first to have a convergence guarantee for solving the TDOA-based geolocation problem under the QP ionosphere model.

IV. Numerical Results

A. Setup

In this section, we present numerical results to demonstrate the efficacy of our proposed approach. The setting of our experiments is as follows. The default ionosphere parameters are $r_m = 6650$km, $y_m = 100$km, and $f_c = 10$MHz. The operating frequency is set at $f = 15$MHz, while the locations of the emitter and sensors are given in Table I. With this setup, we have $L = 849$km and $U = 3059$km for each sensor. The distance between the emitter (in Hong Kong) and

TABLE I
LOCATIONS OF EMITTER AND SENSORS

Emitter	Hong Kong	$114.16°, 22.28°$	β_i
Sensor 1	Beijing	$116.41°, 39.90°$	$6.59°$
Sensor 2	Wuhan	$114.31°, 30.59°$	$25.75°$
Sensor 3	Shanghai	$121.47°, 31.23°$	$15.90°$
Sensor 4	Tokyo	$139.69°, 35.69°$	$0.96°$
Sensor 5	Seoul	$126.58°, 37.33°$	$5.93°$

the furthest sensor (in Tokyo) is 2884km. The measurement noise vector $\boldsymbol{n} = [n_{21}, \ldots, n_{M1}]^T$ is generated according to the Gaussian distribution with mean zero and covariance matrix $\boldsymbol{\Sigma} = 0.5\sigma^2(\boldsymbol{I}_{M-1} + \boldsymbol{e}_{M-1}\boldsymbol{e}_{M-1}^T)$, where σ^2 is the noise power. We consider two scenarios in our experiments. In the first scenario, we use all five sensors to perform the geolocation, while in the second, we use only sensors 1–4. We evaluate the performance of our proposed approach and compare it with that of the approach proposed in [3]. The former applies the GPGD method to problem (4), which explicitly takes the constraints on the flying angles (i.e., $\beta_i \in [0, \beta^{U_1}]$ for $i = 1, \ldots, M$) into account. The latter applies a quasi-Newton (QN) method to a *penalized* version of problem (3), which attempts to control the flying angles via the penalized objective function $\phi(\boldsymbol{\beta}) + \delta \cdot \boldsymbol{e}_M^T \boldsymbol{P}(\boldsymbol{\beta})$. Here, $\delta > 0$ is a penalty parameter. We set $\delta = 0.0001$ in our experiments, as this gives the best performance of the QN method. Both the GPGD and QN methods are run for a maximum of $T = 10^5$ iterations. We have created a graphical user interface to demonstrate the ray paths between the emitter and sensors and the sequence generated by our proposed GPGD method. The source code used to generate the results in this paper can be downloaded at https://github.com/samwong1993/OTHR.

B. Geolocation Performance

Since both problems (3) and (4) are non-convex, the performance of the GPGD and QN methods will in principle depend on the choice of the initial iterate. To study the effect of initialization on the performance of these two methods, we perform two sets of experiments. In the first set, for each noise level $\sigma \in \{0, 100, 200, \ldots, 1000\}$, we generate 100 instances of the geolocation problem with different noise realizations. Then, we initialize both the GPGD and QN methods using the warm-start strategy in [3] and apply these methods to solve the generated instances. The root-mean-square errors (RMSEs) of the two methods are shown in Fig. 3. As can be seen from the figure, our proposed GPGD method not only is more efficient but also achieves a higher geolocation accuracy than the QN method in [3]. For reference, we also include the Cramér-Rao lower bound (CRLB) of the problem in the figure. The derivation of the CRLB can be found in [3].

In the second set, we consider a random initialization strategy. Specifically, for each noise level $\sigma \in \{0, 100, 200, \ldots, 1000\}$, we generate an instance of the geolocation problem and 100 random points to initialize the GPGD and QN methods. Then, we apply the methods to solve the generated instance. The RMSEs of the two methods are shown in Fig. 4. Observe that the RMSE of the GPGD method is comparable to that in Fig. 3. However, the QN method fails

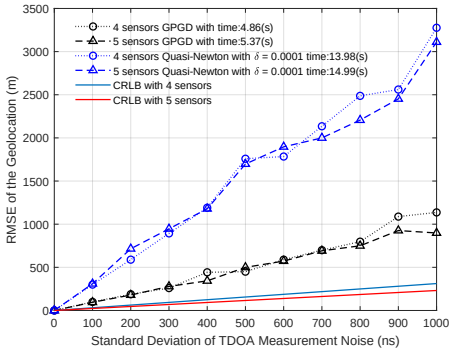

Fig. 3. Geolocation Performance of GPGD and QN: Warm-Start Initialization

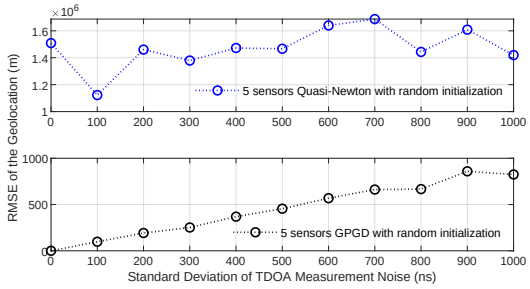

Fig. 4. Geolocation Performance of GPGD and QN: Random Initialization

to geolocate the emitter in this setting (the RMSE is on the order of 10^6m). In Fig. 5, we record the number of initial points (out of the 100 generated) for which the QN method outputs a solution that has an error of more than 50km (i.e., $50,000$m). From the figure, we see that the QN method fails to

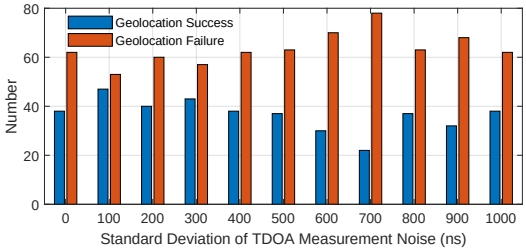

Fig. 5. Geolocation Success Rate of QN with Random Initialization

geolocate the emitter for more than half of the generated initial points. As pointed out in Section III-A, this can be attributed to the ambiguity in the choice of the flying angles during the course of the QN method. We should also remark that the QN method does not have any convergence guarantee. In summary, our proposed GPGD method is much more reliable than the QN method in [3].

V. CONCLUSIONS AND FUTURE WORK

In this paper, we proposed an efficient projected gradient-type method for tackling the TDOA-based geolocation problem under the QP model. The proposed method not only has a provable convergence guarantee but also demonstrates numerical superiority over the existing algorithm in [3]. An interesting future direction is to study the geolocation problem under more realistic ionosphere models.

REFERENCES

[1] A. Jain, P. Pagani, R. Fleury, M. M. Ney, and P. Pajusco, "Efficient time domain HF geolocation using multiple distributed receivers," in *Proceedings of the 2017 11th European Conference on Antennas and Propagation (EuCAP 2017)*. IEEE, 2017, pp. 1852–1856.

[2] ——, "HF source geolocation using an operational TDoA receiver network: Experimental results," *IEEE Antennas and Wireless Propagation Letters*, vol. 17, no. 9, pp. 1643–1647, 2018.

[3] T. Wang, X. Hong, W. Liu, A. M.-C. So, and K. Yang, "Geolocation of unknown emitters using TDOA of path rays through the ionosphere by multiple coordinated distant receivers," in *Proceedings of the 2018 IEEE International Conference on Acoustics, Speech and Signal Processing (ICASSP)*. IEEE, 2018, pp. 3509–3513.

[4] A. H. De Voogt, "The calculation of the path of a radio-ray in a given ionosphere," in *Proceedings of the IRE*, vol. 41. IEEE, 1953, pp. 1183–1186.

[5] T. A. Croft and H. Hoogasian, "Exact ray calculations in a quasi-parabolic ionosphere with no magnetic field," *Radio Science*, vol. 3, pp. 69–74, 1968.

[6] D. Tian, S. Wang, and L. Yang, "Research on the influence of stations distribution to HF TDOA geolocation accuracy," in *Proceedings of the 2018 12th International Symposium on Antennas, Propagation and EM Theory (ISAPE)*, 2018, pp. 1–4.

[7] G. Fabrizio, "Geolocation of HF skywave radar signals using multipath in an unknown ionosphere," in *Proceedings of the 2014 IEEE Radar Conference*, 2014, pp. 0422–0425.

[8] P. Pagani, R. Fleury, Y. Le Roux, and D. Le Jeune, "A study of HF transmitter geolocation through single-hop ionospheric propagation," in *Proceedings of the 2014 8th European Conference on Antennas and Propagation (EuCAP 2014)*, 2014, pp. 2689–2693.

[9] K. Davies, *Ionospheric Radio*, ser. IEE Electromagnetic Waves Series. Peter Peregrinus Ltd., 1990, vol. 31.

[10] G. Wang, A. M.-C. So, and Y. Li, "Robust convex approximation methods for TDOA-based localization under NLOS conditions," *IEEE Transactions on Signal Processing*, vol. 64, no. 13, pp. 3281–3296, 2016.

[11] K. Yang, L. Jiang, and A. M.-C. So, "A semidefinite relaxation approach to the geolocation of two unknown co-channel emitters by a cluster of formation-flying satellites using both TDOA and FDOA measurements," in *Proceedings of the 2016 IEEE International Conference on Acoustics, Speech, and Signal Processing (ICASSP 2016)*, 2016, pp. 2911–2915.

[12] H. Liu, Y.-M. Pun, and A. M.-C. So, "Local strong convexity of maximum-likelihood TDOA-based source localization and its algorithmic implications," in *Proceedings of the IEEE 7th International Workshop on Computational Advances in Multi-Sensor Adaptive Processing (CAMSAP 2017)*, 2017, pp. 1–5.

[13] J. Nocedal and S. J. Wright, *Numerical Optimization*, 2nd ed., ser. Springer Series in Operations Research and Financial Engineering. Springer Science+Business Media LLC, 2006.

[14] G. S. Sales, "High frequency (HF) radiowave propagation," *Scientific Report #6, PL-TR-92-2123, Phillips Laboratory*, 1992.

[15] Z.-Q. Luo, W.-K. Ma, A. M.-C. So, Y. Ye, and S. Zhang, "Semidefinite relaxation of quadratic optimization problems," *IEEE Signal Processing Magazine*, vol. 27, no. 3, pp. 20–34, 2010.

[16] A. M.-C. So and Y. Ye, "Theory of semidefinite programming for sensor network localization," *Mathematical Programming, Series B*, vol. 109, no. 2, pp. 367–384, 2007.

[17] K. W. K. Lui, W.-K. Ma, H. C. So, and F. K. W. Chan, "Semi–definite programming algorithms for sensor network node localization with uncertainties in anchor positions and/or propagation speed," *IEEE Transactions on Signal Processing*, vol. 57, no. 2, pp. 752–763, 2009.

[18] A. N. Iusem and A. R. de Pierro, "On the convergence properties of Hildreth's quadratic programming algorithm," *Mathematical Programming*, vol. 47, pp. 37–51, 1990.

[19] A. S. Lewis, D. R. Luke, and J. Malick, "Local linear convergence for alternating and averaged nonconvex projections," *Foundations of Computational Mathematics*, vol. 9, pp. 485–513, 2009.

[20] H. Attouch, J. Bolte, and B. F. Svaiter, "Convergence of descent methods for semi-algebraic and tame problems: Proximal algorithms, forward-backward splitting, and regularized Gauss-Seidel methods," *Mathematical Programming*, vol. 137, no. 1-2, pp. 91–129, 2013.